

Article

Understanding Wave Attenuation Across Marshes: Insights from Numerical Modeling

Madeline R. Foster-Martinez ^{1,*} , Ioannis Y. Georgiou ² , Duncan M. FitzGerald ³ , Zoe J. Hughes ³ , Alyssa Novak ³ and Md Mohiuddin Sakib ¹

¹ Earth and Environmental Sciences, University of New Orleans, New Orleans, LA 70148, USA; msakib@uno.edu

² Coastal and Deltaic Systems Modeling, The Water Institute, New Orleans, LA 70122, USA; igeorgiou@thewaterinstitute.org

³ Earth and Environment, Boston University, Boston, MA 02215, USA; dunc@bu.edu (D.M.F.); zoeh@bu.edu (Z.J.H.); abnovak@bu.edu (A.N.)

* Correspondence: mrfoster@uno.edu; Tel.: +1-504-280-4747

Abstract: Marsh vegetation dampens wave energy, providing protection to coastal communities from storms. A new modeling framework was applied to study wave height evolution over the saltmarsh bordering Newbury, MA. A regional Delft3D hydrodynamic model generated wind driver waves in the open water portions of the study area, which were then one-way coupled with an analytical model, the Marsh Transect Wave Attenuation (MTWA) model, which tracked wave evolution along select transects throughout the marsh. Field observations of vegetation and wave height evolution were used to calibrate MTWA. Seven scenarios were run covering a range of possible future management and environmental conditions, in addition to projected sea level rise. Results underscore the importance of vegetation and elevation to wave attenuation.

Keywords: coastal protection; wave attenuation; saltmarsh; Delft3D; *Spartina alterniflora*; *Spartina patens*; transect model; storm surge; sea level rise; vegetation



Academic Editor: Wei-Bo Chen

Received: 26 April 2025

Revised: 6 June 2025

Accepted: 10 June 2025

Published: 18 June 2025

Citation: Foster-Martinez, M.R.; Georgiou, I.Y.; FitzGerald, D.M.; Hughes, Z.J.; Novak, A.; Sakib, M.M. Understanding Wave Attenuation Across Marshes: Insights from Numerical Modeling. *J. Mar. Sci. Eng.* **2025**, *13*, 1188. <https://doi.org/10.3390/jmse13061188>

Copyright: © 2025 by the authors. Licensee MDPI, Basel, Switzerland. This article is an open access article distributed under the terms and conditions of the Creative Commons Attribution (CC BY) license (<https://creativecommons.org/licenses/by/4.0/>).

1. Introduction

Salt marshes are highly valued because they provide wide benefits to the marine ecological community [1], as well as protecting the mainland during major storm events by reducing surge and the effects of damaging waves [2]. The level of protection is variable and depends on many factors including: 1. storm intensity, 2. wind direction, 3. timing with respect to tidal elevation, 4. vegetation type, health, and seasonal elevation and density, and 5. characteristics of the marsh edge (the height, slope, and width of fronting tidal flat) as well as the bathymetry and extent of the adjacent open-water area. Like many marshes in coastal plain settings [3], the Great Marsh behind Plum Island in the Merrimack River Embayment (Figure 1) borders several towns, penetrating deeply into town interiors at a number of locations. Moderate to large extratropical storms frequently cause flooding in these communities, which is exacerbated during intense precipitation events, and in the long term by accelerating sea-level rise (e.g., [4]). The higher occurrence of extratropical storms in New England [5,6] is leading to more frequent coastal flooding and greater wave erosion, particularly during periods of large astronomic tides. For example, slow moving storms in January and March of 2018 contained gale-force winds with gusts greater than 60 mph, producing two of the three highest storm surges ever recorded in nearby Boston Harbor [7]. Predicted SLR and increased storm surge elevations have the potential to significantly impact coastal economies, facilities, and infrastructure.

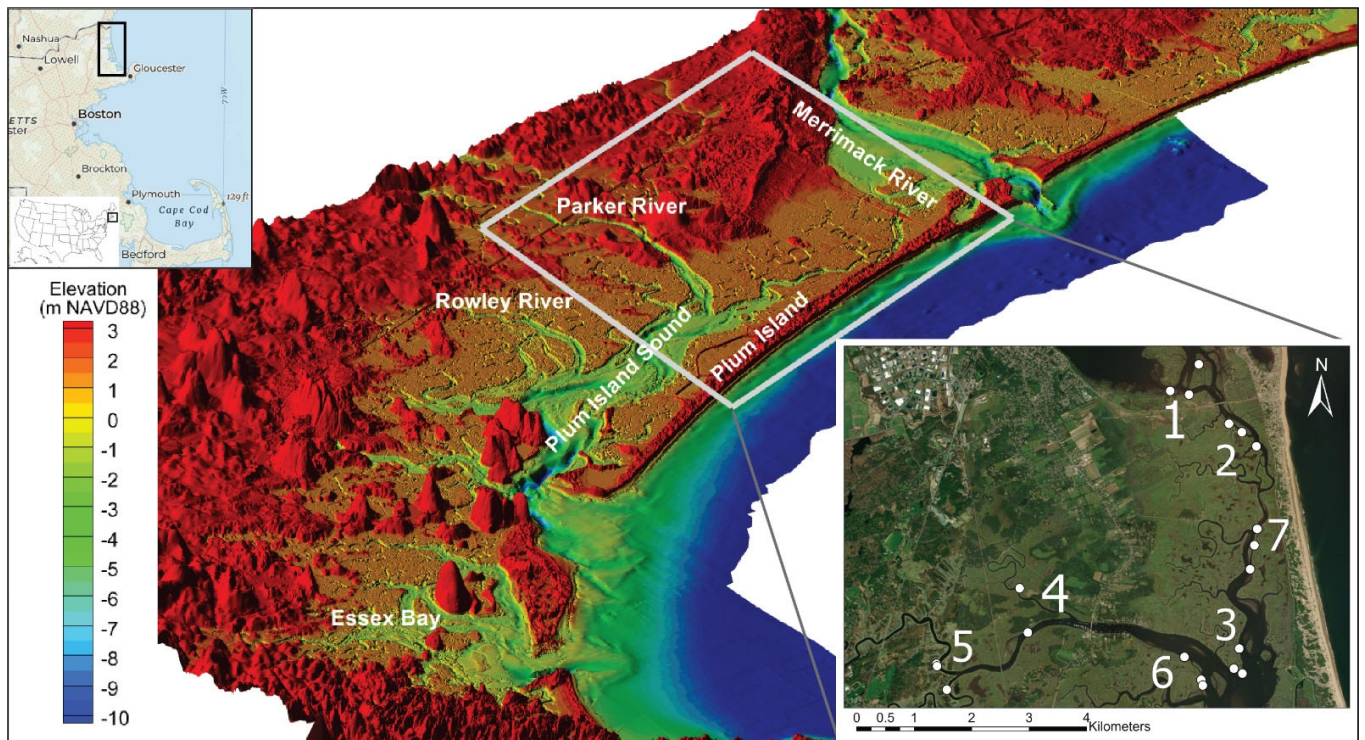


Figure 1. Digital elevation map of the study area with respect to m NAVD88. The position of the field site within the Gulf of Maine coast and within the United States is shown in the upper left box. The white square and inset aerial photograph (imagery copyright 2023 Maxar) depict the seven areas of interest (numbered in white). White dots indicate where wave data were evaluated in the attenuation model (MTWA).

Here, we explore how the marsh platform in the Great Marsh, Massachusetts, will affect wave energy, particularly during storms, in a regime of accelerating SLR. Wave processes at the edge of the marsh platform have been extensively investigated at the Great Marsh [8–11]. Likewise, wave attenuation has been analyzed at specific marshes in field experiments [12,13] and in lab experiments [14]. In this study, we examine the timescale of a storm and how wave propagation changes under different storm magnitudes and SLR conditions, including the effects of concentrated wave activity on specific marsh environments. We do this by coupling a numerical model with an analytical model—calibrated with field data to predict wave characteristics—and apply it to seven study sites within the Great Marsh in northern Massachusetts. Because wave attenuation is not a constant process, our modeling includes multiple scenarios using different hydrodynamic conditions produced by variable storms, water levels, and rates of SLR. Additionally, modeling allows us to explore possible outcomes for different intervening human actions and environmental conditions. Understanding the current protection provided by the adjacent marshlands and how this sheltering may change is key to preparing for future conditions and increasing resiliency.

Physical Setting

The backbarrier of Plum Island is dominated by an elongate, north–southward trending shallow lagoonal estuary floored by intertidal and subtidal sand shoals. Mean depth along the thalweg gradually deepens from less than 2 m in the upper northern section of Plum Island Sound to greater than 10 m at the mouth (Figure 1). Extensive wetlands border the estuary, particularly to the north and west. The region experiences semi-diurnal tides with a mean range of 2.8 m, increasing to more than 3.7 m during perigean spring

tidal conditions [15]. The vast majority of the backbarrier tidal prism ($32 \times 10^6 \text{ m}^3$ [16]) is exchanged through the Plum Island Sound inlet at the southern end of Plum Island, with some additional tidal water discharged into the Merrimack Estuary through Plum Island creek ($2.3 \times 10^6 \text{ m}^3$ [17]).

Our study site, in the northern portion of the estuary, consists of broad platform marshes dissected by several major channels including the Parker and Plum Island Rivers and several smaller creeks (Figure 1). The high marsh is dominated by *Spartina patens* and *Distichlis spicata*, and the less extensive low marsh is vegetated by short-form *Spartina alterniflora*. Long- and short-form *Spartina alterniflora* are typically found along creek banks and in poorly drained areas, respectively [18]. Low marsh areas have an average elevation of 0.98 m above mean sea level; high marshes are about 40 cm higher and flood only during spring tides [19,20]. Tidal channels and anthropogenic ditches dissect the entire marsh and numerous large and small salt pannes and ponds spot the high marsh surface. Seven representative marsh sites were selected throughout the study site and used as a framework for analyzing model results (Figure 1). These sites were chosen to cover a range of exposures to the magnitude and direction of wave energy and had similar vegetation characteristics.

2. Methods

We used a regional-to-local approach to evaluate wind-generated waves in Plum Island Sound and assess wave attenuation on the marsh surface (similar to frameworks in [21,22]). At the basin scale, a hydrodynamic model previously validated with deployments in Plum Island Sound was used to simulate surge and wind-generated waves (see [7]). At selected locations in the basin, output from the regional model was used to inform a local high-resolution wave model along the marsh platform (Marsh Transect Wave Attenuation Model (MTWA)), to better capture drivers, feedback, and controls on wave attenuation along the marsh platform.

2.1. Data, Observations, and Analysis

2.1.1. Bathymetry and Topography

The model utilizes recent bathymetry available for the area and included the following: (1) regional bathymetry for the coastal ocean based on the Coastal Relief Model from NOAA [23], (2) regional LiDAR obtained from the US Army Corps of Engineers [24], and (3) additional single-beam bathymetry (Teledyne Marine RiverRay Acoustic Doppler Current Profiler – ADCP, Daytona Beach, FL, USA) with integrated real time kinematic (RTK) differential Global Positioning System (GPS; Hemisphere V200 DGPS, Scottsdale, AZ, USA) observations taken during the a previous study following Hurricane Sandy funded by the National Fish and Wildlife Foundation (NFWF) in Plum Island Sound in 2015, to resolve smaller tidal channels and marsh edge topography. Marsh surface elevations for future SLR scenarios evaluated during the study were determined using projections of the marsh surface from accretion measurements from the same study, where 15 cores throughout the great marsh were collected and analyzed for accretion using ^{210}Pb and ^{137}Cs [25].

2.1.2. Vegetation

Vegetation was mapped along three transects at each of the seven sites using a Trimble model 5800 RTK differential GPS (Westminster, CO, USA). Each transect was oriented to run from the edge of a creek/water body toward the upland border with sampling occurring at 100 m intervals. At each sampling location, a GPS point and an elevation measurement were recorded. In addition, vegetation attributes (species composition, percent cover, canopy height, and shoot density) were collected using a 0.5 m² quadrat and the habitat type (e.g., creek edge, low marsh, high marsh, pool, panne, or upland) was described. Areas

along the transect containing $> 1.0 \text{ m}^2$ of invasive vegetation (e.g., *Leipidium densiflorum*, *Phragmites australis*) were delineated, as well as regions experiencing changes in species composition due to increased tidal inundation. The type and character of the vegetation was used to inform the MTWA model, but not the Delft3D model.

2.2. Regional Hydrodynamic Modeling

The use of wave models in coastal systems depends largely on the application. In settings where wave reflections are present such as in harbors, near coastal structures (e.g., breakwaters, seawalls, and other structures), where ship-wakes are of concern, and along rocky coastlines, Boussinesq models (e.g., FUNWAVE; [26,27]) are often used [28,29]. These applications require fully non-linear models that can capture irregular waves, the effects of wave reflections accounting for Bragg resonant conditions and Bragg reflection [30,31]. Plum Island has a large embayment flanked by marshes, and the absence of structures, rocks, or other conditions allows for a reasonable representation of the incident waves using spectral waves.

For wave generation and propagation within the Plum Island embayment, we used the Delft3D modeling suite [32], a numerical process-based model that can resolve hydrodynamics (flow, D-FLOW, and waves, D-WAVES, which is based on SWAN; [33]), sediment transport, and resulting morphology under the combined effects of currents and waves, and that is widely used in coastal systems (e.g., [34–38]). The resolution of the regional grid (flow) for Plum Island Sound varied from 2 to 3 km offshore to 20 m in the vicinity of tidal inlets and throughout the backbarrier, while the regional grid for waves had similar resolution offshore but was 60 m throughout the sound. Storm wave propagation used the third-generation wave model SWAN [33] within the Delft3D modeling suite and included wind growth to accurately simulate water level setup (increase storm surge elevation) due to waves.

2.2.1. Boundary Conditions

For tidal conditions at the open marine boundary, we used tidal constituents from the East Coast tidal database [39]. For the selected storms used in the analysis, we used a time series of storm surges and waves, from the North Atlantic Coastal Study (NACCS) [40], as well as a re-analysis of storms from the Wave Information Study (WIS) [41]. Winds and waves at the open boundary also leveraged the above studies (i.e., NACCS and WIS).

2.2.2. Calibration and Validation

The model was previously validated for tidal hydrodynamics using observations from deployments throughout Plum Island in 2015 [7]. The regional wave model was validated using a nearshore ($\sim 10 \text{ m}$) deployment northeast of the tidal inlet in Plum Island during the same campaign. The model was tuned to reproduce observed conditions by an adjustment of the bottom friction term.

2.2.3. Storm Characterization and Analysis

To select a suite of storms to run in the model, we used WIS station 63045 located in 85 m of water depth east–northeast of Plum Island. Our analysis of all events in the record shows that our study site is exposed to storms with wind and waves from ~ 20 to 180° azimuth, with additional exposure to high fetch conditions from 20 to 135° . The most frequent events occur from 78 to 145° , and the top ten events on record were from 61 to 101° . Hence, we selected four of the top ten events to simulate for our analysis (Table 1). For each of these events, the wind speed, direction, offshore wave height and wave period, and corresponding surge from NACCS, was forced at the open boundary.

Table 1. Storm event analysis conducted by the US Army Corps of Engineers at WIS station 63045. The table shows the events selected from the top ten ranked by H_{mo} .

Event	Date	Time (UTC)	H_{mo} (m)	T_{peak} (s)	θ_{mean} *
4	16 January 1980	12:00	6.37	12.79	80.0
5	14 March 2010	15:00	6.11	12.08	99.0
6	12 December 1992	08:00	6.08	12.77	93.0
7	9 February 2013	03:00	5.86	10.81	61.0

* Direction that waves are arriving from.

2.3. Marsh Transect Wave Attenuation Modeling

The MTWA model is a stand-alone wave attenuation model for coastal marshes that operates on a shore-normal transect. It computes the evolution of wave heights along the transect as a wave progresses from open water, over the marsh edge, and across the marsh platform, and was calibrated with observations at the site (Supplemental Information). MTWA includes four processes, which transform the wave height: interaction with scarps, shoaling, drag from bottom roughness, and drag from vegetation. The model does not include wave setup or wave regeneration due to wind, which could cause greater wave propagation. MTWA evaluates cell by cell based on the underlying digital elevation model (DEM). The DEM used here has a resolution of 1 m, and therefore, the MTWA resolution is also 1 m. It is a one-dimensional model (i.e., the cell does not have a width). The MTWA model was one-way coupled to the Delft3D model, which provides input information on the wave characteristics and water level at the start of the transect (similar framework as [42,43]). A conceptual diagram listing the criteria for determining the processes within each cell is given in Figure 2, and more detail on each step is provided below.

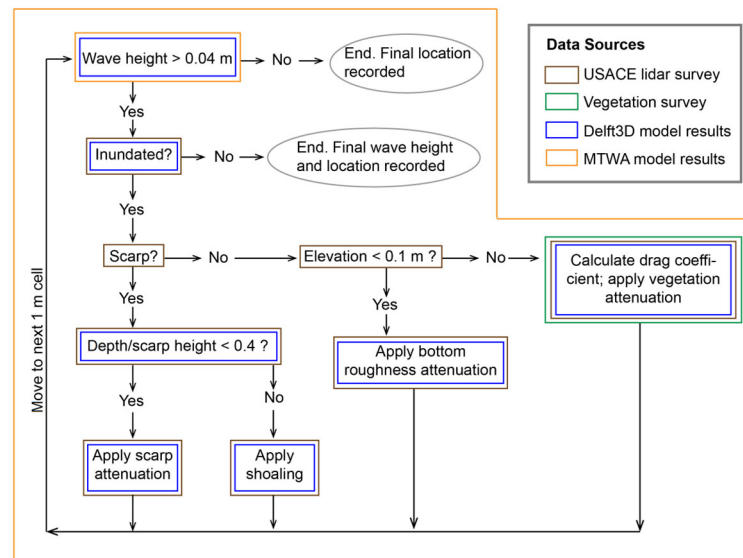


Figure 2. Conceptual diagram of the Marsh Transect Wave Attenuation (MTWA) model. The color of the box indicates the source of data inputs for that step. Elevation data reference: m to NAVD88.

2.3.1. Interactions with Scarps and Shoaling

If a cell is inundated, the elevation change between the previous cell and current cell is calculated. If the elevation difference between these two cells exceeds 0.6 m, it is determined to be a scarp. This threshold is an estimate based on observations in the field, as well as data used to classify stable or accretionary marsh edges versus slumping or vertical and abrading edges in Houttuijn Bloemendaal et al. [10]. If the ratio of the cell depth to the

scarp height is less than 0.4 (i.e., the upper limit of our observations shown in Figure 3), the following relationship is applied:

$$H = H_0 \times d \times 2.366 \left(\frac{h}{h_{scarp}} \right)^{1.698} \tag{1}$$

where h_{scarp} is the height of the scarp, H_0 is the wave height in the previous cell, d is the distance across the scarp, and H is the wave height in the current cell. This empirical relationship was formulated from the wave data collected in this study (Supplemental Information).

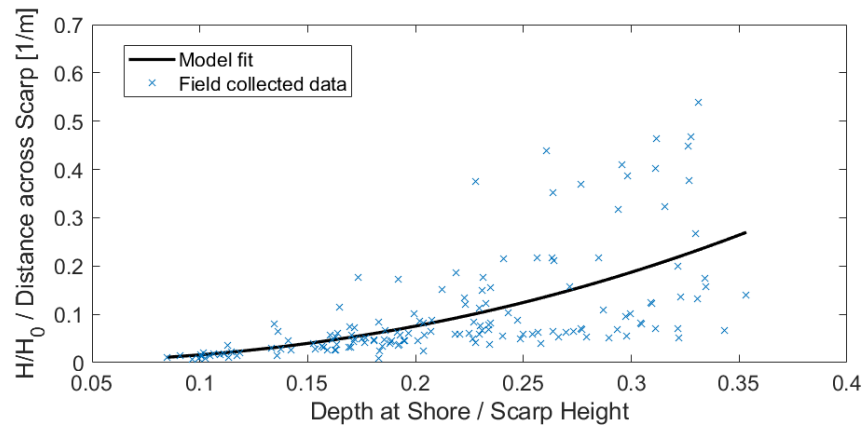


Figure 3. Empirical model used for wave transformation over a marsh scarp.

If the ratio of the cell depth to the scarp height is greater than 0.4, shoaling is applied as follows [44]:

$$H = H_0 \left(\frac{h_0}{h} \right)^{\frac{1}{4}} \tag{2}$$

where h is the water depth and h_0 is the water depth in the previous (seaward) cell.

2.3.2. Bottom Roughness

If the elevation of the cell is less than 0.1 m NAVD88 and it was determined to not be a scarp, then drag from bottom roughness is applied, and the wave height is decreased. The drag from bottom roughness is calculated for a flat bottom slope following [44]:

$$K_f = \left[1 + \frac{8f_w}{6\pi} \frac{k^2 H_0 \Delta x}{(2kh + \sinh(2kh)) \sinh(kh)} \right]^{-1} \tag{3}$$

where k is the wave number, and f_w is the wave friction factor defined as follows [45]:

$$f_w = \exp \left[5.213 \left(\frac{2\pi k_b}{Tu_B} \right)^{0.194} - 5.977 \right] \tag{4}$$

where k_b is the roughness length scale, which was set to 0.01, and T is the wave period. The wave height is then calculated as follows:

$$H = H_0 K_f \tag{5}$$

2.3.3. Drag Due to Vegetation

If the elevation is greater than 0.1 m NAVD88, and it was determined to not be a scarp, then it is considered vegetated (i.e., marsh). First, the stem Reynolds number, Re , is calculated from the inputs from Delft3D and the vegetation survey:

$$Re = \frac{u_b b_v}{\nu} \tag{6}$$

where ν is kinematic viscosity (m^2/s), u_b is the bottom orbital velocity (m/s), and b_v is the stem diameter (m). The drag coefficient, C_D , is calculated as follows and shown in Figure 4:

$$C_D = -0.528 + \left(\frac{222.4}{Re}\right)^{0.804} \tag{7}$$

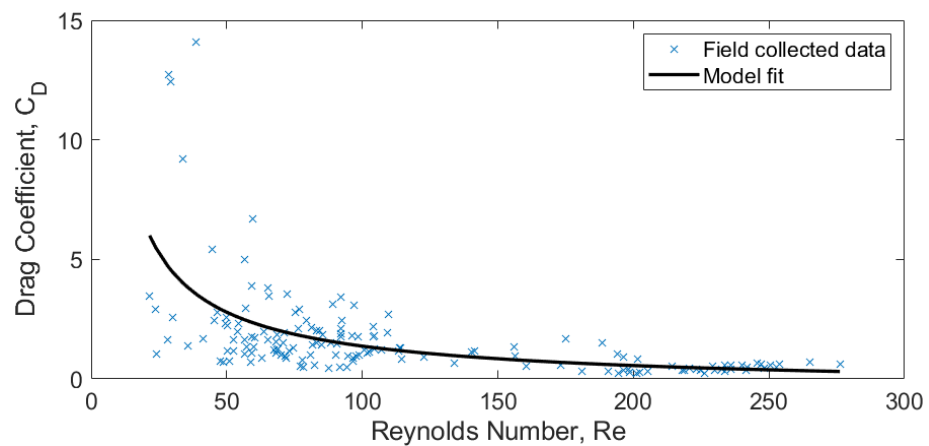


Figure 4. Relationship between Reynolds number, Re , and drag coefficient, C_D , from field data (blue x) and model fit (black line). As the Re gets larger, the drag coefficient decreases. For values of Re outside of these bounds, constant values are used in the MTWA model. The lowest C_D value measured was 0.21, and the largest was 14.

This relationship was derived from field observations of wave height transformation across the marsh in the study area (Areas 1 and 3 in Figure 1). Instruments collected data from 27 November 2018 to 7 January 2019, at three stations along three cross-shore transects. There were two tidal cycles where wave heights were between 0.1 and 0.2 m and water depths on the marsh platform were 0.6–0.8 m. The remaining observations were of calmer conditions with wave heights less than 0.1 m.

Equation (7) is used for values of Re in the range of those observed during the field campaign. For Re below 21, C_D is set to 6 (minimum from field observations), and for those above 390 (maximum from field observations), it is set to 0.2. The drag coefficient is then used as follows to calculate the wave height in the given cell:

$$H = \frac{H_0}{1 + \tilde{\beta}x} \tag{8}$$

where

$$\tilde{\beta} = \frac{1}{3\sqrt{\pi}} C_D b_v N H_0 k_p \frac{\sinh^3 k_p \alpha h + 3 \sinh k_p \alpha h}{(\sinh 2k_p h + 2k_p h) \sinh k_p h} \tag{9}$$

N is the number of vegetation stems in a square meter (m^{-2}), α is the ratio of the water depth to the vegetation height (h_v/h), and k_p is the wave number.

2.4. Model Runs

Each of the four selected storms were run under two tide conditions, spring high tide (herein “high”) and neap high tide (herein “low”), as well as with and without additional SLR, creating a total of 16 Delft3D runs with different hydrodynamic conditions. The MTWA was applied to three transects within each of the seven areas of interest (Figure 1). The three transects chosen are representative of conditions of that area. For each of the 16 runs, the conditions with the largest wave that occurred at the start of each transect were extracted and used as input to the MTWA model with base conditions (Table 2, scenario 1). Base conditions reflect average conditions observed during the field campaign (Supplemental Information), average properties for vegetation, and an unaltered DEM. Additional runs were conducted where base conditions along the MTWA transects were manipulated to reflect six additional environmental scenarios identified in discussion with community stakeholders (Table 2, scenarios 2–7). These six scenarios were run using non-SLR inputs from the Delft3D runs.

Table 2. Environmental scenarios and implementation descriptions for MTWA.

Scenario	Parameters Used and/or Altered
1. Base	Average vegetation characteristics; unaltered DEM
2. All <i>Spartina alterniflora</i>	<i>Spartina alterniflora</i> characteristics; unaltered DEM
3. All <i>Spartina patens</i>	<i>Spartina patens</i> characteristics; unaltered DEM
4. Tidal flat	Vegetation drag switched off; unaltered DEM
5. Tidal flat, lower elevation	Vegetation drag switched off; DEM lowered
6. Lower elevation	Average vegetation characteristics; DEM lowered
7. Ditches filled	Average vegetation characteristics; elevation of ditches increased

2.4.1. Environmental Scenarios

For the *Sp. alterniflora* and *Sp. patens* cases (scenarios 2 and 3), vegetation parameters in the vegetation drag model (Equations (6)–(9)) were altered to reflect *Sp. alterniflora* (less stem density, N , and larger stem width, b_v) and *S. patens* (greater stem density, N , and smaller stem width, b_v). The values were taken from survey plots that contained over 50% of these species (Supplemental Information).

To examine the conversion to a tidal flat, MTWA was run without the vegetation drag option to simulate no vegetation (scenarios 4 and 5). For the tidal flat, lower elevation, the marsh platform was lowered by 10% and the vegetation option remained off. To test only a lower elevation, the platform was lowered by 10% with the vegetation drag option on (scenario 6).

The study area contains drainage ditches, which segment the marsh platform while increasing rate of tidal exchange. Managers have proposed filling the ditches as a means of returning the marsh to its pre-anthropogenic condition and reestablishing the original marsh hydrology. To simulate ditch filling, the DEM was altered prior to input into MTWA (scenario 7). Cells with elevation less than 0.8 m NAVD88 on the marsh platform were raised to the average elevation of the cells 3 m away in both the seaward and landward directions. If more than three consecutive cells were below 0.8 m NAVD88, it was identified as a channel (i.e., not a ditch), and the elevation was not changed. This elevation, 0.8 m NAVD88, was identified as being the threshold for ditches.

2.4.2. Adjustment of Marsh Platform Due to Sea Level Rise

Forward projection indicates a very likely 21st century global sea level (GSL) rise of around 135 cm under maximum range across all RCP scenarios [46]. We updated our

existing bathymetry by incorporating an extreme projection of 21st century GSL rise to evaluate future sea level rise impact on the Plum Island backbarrier marsh in 2100. Average marsh accretion in Plum Island is ~2.8 mm/yr based on measurements obtained during an earlier study [7]. The GSL rise rate at Plum Island is 2.85 mm/yr. We have calculated the time varying acceleration rate for the extreme sea level rise projection from [46] and added that acceleration rate on both GSL rise as well as marsh accretion rate. We considered hundred percent of that constant acceleration for each future year projection of GSL rise and only seventy percent acceleration on marsh accretion. We assumed that the marsh could accrete a maximum of 7 mm/yr in future and five times more than the open-water body, which was updated in our bathymetry calculation:

For marsh or any land,

$$Z_{final} = Z_i + (GSLR + Acr) \quad (10)$$

For open water,

$$Z_{final} = Z_i + (GSLR + Acr/5) \quad (11)$$

where, Z_{final} = final depth;

Z_i = initial depth;

GSLR = global sea level rise rate in meter/yr;

Acr = accretion rate in meter/yr.

3. Results

3.1. Largest Wave Heights at the Marsh Edge

Due to the variation in directions of approach, each storm impacted the areas of interest differently. By examining the percent change in the largest wave heights at each transect, we can understand how the wave conditions may change throughout the region with SLR and tide levels. For each Delft3D model run, the waves within the areas of interest were averaged together. The percent change was calculated comparing the same storm and area of interest but with different tide or SLR cases. The percent change was then averaged across the areas of interest and for the four different storms to produce average changes for the following four comparisons: (1) impact of SLR at high tide, (2) impact of SLR at low tide, (3) impact of the tide case without SLR, and (4) impact of the tide case with SLR.

The largest change was a $44\% \pm 4\%$ increase in wave heights for the low tide case with and without SLR. Wave heights only increased by $23\% \pm 1\%$ for the high tide case with and without SLR. Since the area is already inundated to a greater extent during high tide, the additional inundation from SLR does not cause as large of an increase in wave heights. There is less difference between the low and high tide cases. With SLR, the wave heights were $26\% \pm 2\%$ greater at high tide than low tide, and without SLR, they were $31\% \pm 6\%$ greater.

3.2. Wave Attenuation

The distance needed for complete wave attenuation is a good metric of the level of coastal protection provided. The longer distance required indicates waves are encroaching farther inland. We defined complete attenuation within the MTWA model as the point when the wave height is 0.04 m or less. The distance from the start of the transect to complete attenuation was recorded and compared for the different scenarios (Table 2). For some conditions, complete attenuation was not achieved. This occurred due to one of three reasons: the wave reached a higher elevation (i.e., upland) where the marsh was no longer inundated; the wave height never decreased to 0.04 m across the 1000 m transect; or the Delft3D output had no wave activity at that location.

The marsh width was sufficient to achieve complete attenuation in most locations and scenarios. For the base high tide case without SLR, the waves were completely attenuated before reaching the upland surrounding the marsh, except in two areas: Areas 1 and 5. At these sites, wave heights were reduced from 0.53 m to 0.05 m and 0.26 m to 0.07 m, respectively. The resulting breaking waves against the shore were very small, but not completely attenuated because the marsh is quite narrow at these sites.

For comparison among the scenarios, an averaging scheme similar to the one for wave heights at the marsh edge (described in Section 3.1) was conducted. Complete attenuation distance was first averaged across the transects in each area of interest. Those values were used to calculate the percent change per storm and per area of interest. The percent change was then averaged across the areas of interest and storm, in that order. The results are shown in Figure 5 and referenced in the subsections below.

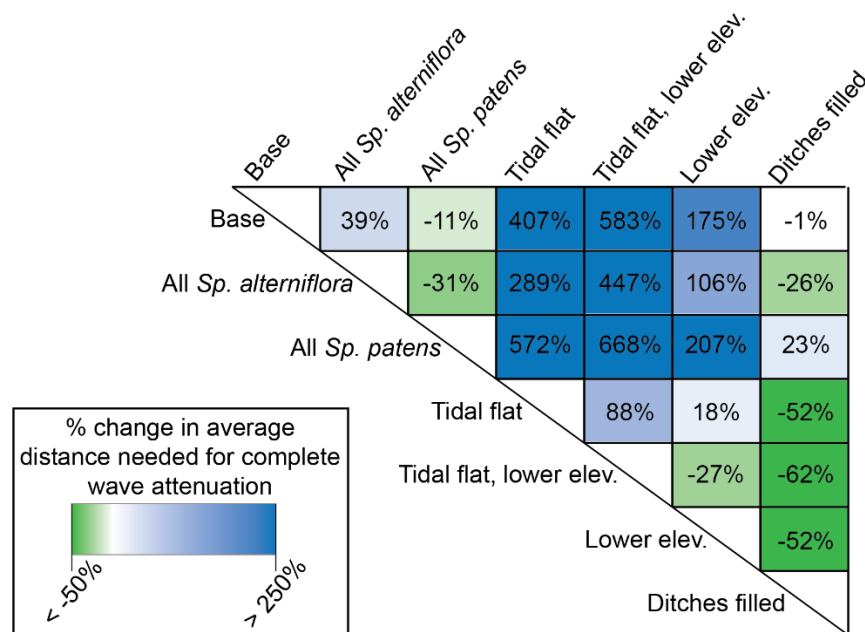


Figure 5. The percent difference in distance to complete wave attenuation between different modeled environmental scenarios. Scenarios in the rows are compared against those in the columns (e.g., compared to the base case, changing the vegetation to all be *Spartina alterniflora* increases the distance needed for complete wave attenuation by 39% (value on the top left)). Details of the scenarios are given in Table 2.

3.2.1. Sea Level Rise

The results with SLR show greater inundation than those without, as expected. Greater inundation leads to less attenuation by vegetation. However, the Delft3D simulations show that the waves generated in the model with SLR tend to have longer wavelength (i.e., smaller wave number) and greater height. If all other conditions are held constant, vegetation attenuates waves with longer wavelengths to a greater degree than shorter wavelengths and attenuates larger wave heights more rapidly than smaller wave heights (on a percentage basis). These effects are competing and depend on the degree of difference in the inundation, wavelength, and wave height. The waves with SLR reach a height of 0.04 m closer or farther from the marsh edge than the waves without SLR.

While on average the distance to complete attenuation was 47% ± 5% greater with SLR with high tide inundation compared to without, local conditions impact the magnitude and direction of this difference. Figure 6A,B show example transects where waves persisted for a greater distance primarily due to the increased inundation with SLR. The vegetation in Area 2 (Figure 6A) filled most of the water column with or without SLR. Therefore, the

difference between the two cases was negligible, and the waves attenuated less than 25 m into the marsh. In Area 1 (Figure 6B), the water was deeper, and there was a 55 m difference in the distance to complete attenuation. Area 7 is an example of where attenuation distance is sensitive to storm direction and wave period. Figure 6C shows the outcome for storm 7, which approached from the east–northeast; the longer wave periods generated with SLR caused a shorter attenuation distance than without SLR. The opposite was true for the same location with storm 6, which approached from the east–southeast. Regardless, these differences are small, less than 5 m.

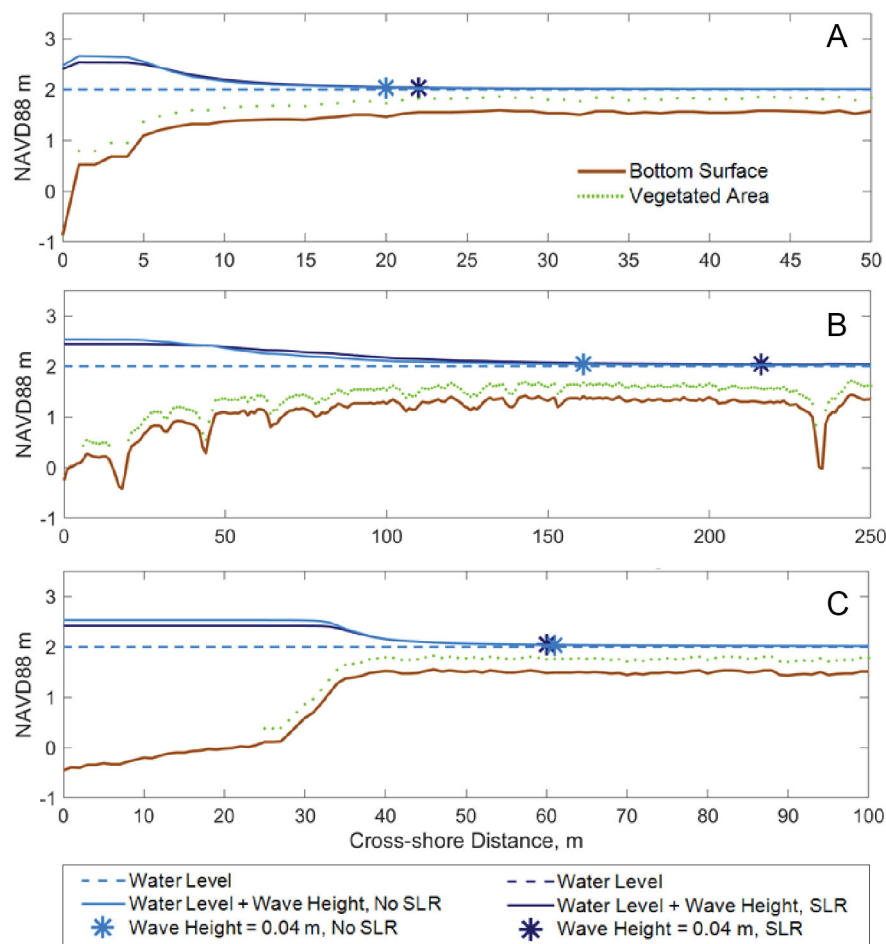


Figure 6. Wave height change from open water (left) to vegetated marsh (right) with SLR (dark blue) and without SLR (light blue) for three example transects in different areas of interest: (A) Area 2, transect 3, storm 7; (B) Area 1, transect 3, storm 7; and (C) Area 7, transect 3, storm 7. All are with high tide conditions. Complete wave attenuation is defined as a wave height of 0.04 m or less and is marked by the asterisk. Refer to Figure 1 for locations of areas of interest.

3.2.2. Vegetation Type

Spartina alterniflora and *Spartina patens* are two common marsh vegetation species with different morphologies. While complete conversion to either type is not likely, increased inundation leads to the encroachment of *Spartina alterniflora* on *Spartina patens* [47]. *Spartina patens* is shorter and has thinner stems in more dense stands of vegetation than *Spartina alterniflora*. *Spartina alterniflora* has two forms: a short form that grows on the marsh platform and a long form that grows at the mid-tide level and populates tidal creeks and tidal flats. Here, we see these differences impact the wave attenuation in different ways depending on the hydrodynamics. The drag coefficient is determined by Re , and Re is directly proportional to the stem width. Therefore, *Spartina patens* tends to have a lower Re and higher drag coefficient than *Spartina alterniflora*. On average, the waves on transects

modeled with all *Spartina patens* reached complete attenuation over a $31\% \pm 2\%$ shorter distance than with all *Spartina alterniflora* (Figure 5). However, there were cases where the reverse was true. This outcome occurred when the limits of the drag coefficient were reached (described in Section 2.3.3), and the competing impacts of stem width, density, and height (compared to water depth) impacted the outcome.

The impact of the larger drag coefficient with *Spartina patens* was greater, and on average, compared to the base case, converting all vegetation to all *Spartina patens* caused an $11\% \pm 3\%$ decrease in distance to complete wave attenuation (Figure 5). *Spartina alterniflora* had the reverse outcome compared to the base case, and on average, the distance to complete wave attenuation increased on average by $39\% \pm 4\%$.

3.2.3. Conversion to Tidal Flat

Removing drag due to vegetation produced dramatically different results. In the absence of vegetation, only drag due to bottom roughness reduces wave height. Without vegetation, 65% of the transects did not reach complete attenuation, whereas with vegetation only 15% did not reach complete attenuation across all four storms simulated. For those that did reach complete attenuation, the distance required was on average $407\% \pm 12\%$ greater than the base case (Figure 5). Figure 7A is an example case with complete attenuation occurring within 22 m of the marsh edge with vegetation and 191 m without vegetation.

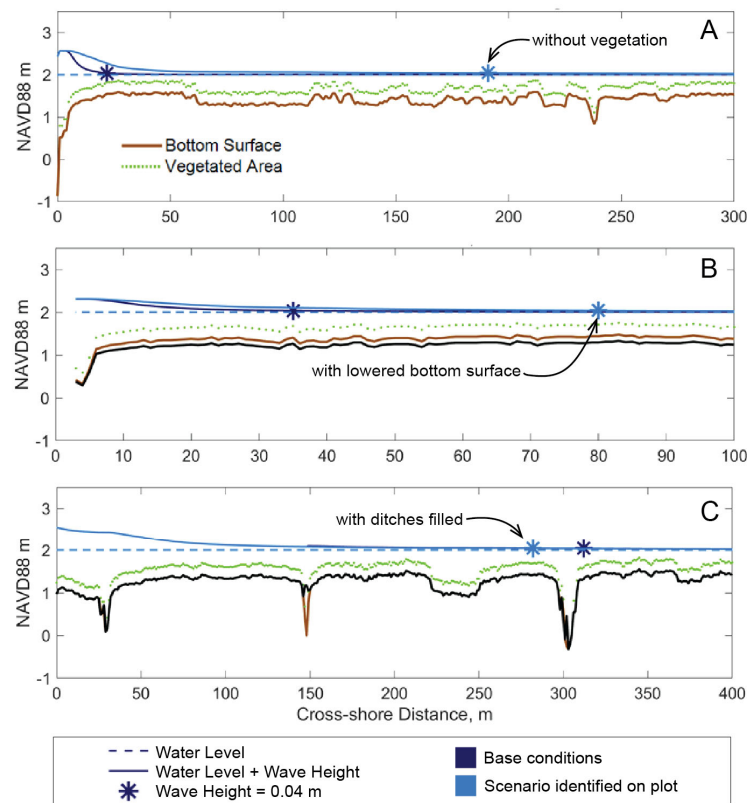


Figure 7. Wave height change from open water (left) to vegetated marsh (right) with base conditions (dark blue) versus environmental scenarios (light blue): (A) no vegetation (scenario 4) at area 2, transect 3, storm 4; (B) a lower elevation (scenario 6) at area 5, transect 2, storm 7; and (C) ditches filled (scenario 7) at area 6, transect 2, storm 6. Brown lines are the base case bottom surface, and black lines are the adjusted bottom surfaces (B,C). Complete wave attenuation is defined as a wave height of 0.04 m or less and is marked by the asterisk. Refer to Figure 1 for locations of areas of interest.

3.2.4. Conversion to Tidal Flat with Lower Elevation

Platform elevation has an important impact on wave energy, as lower elevation creates deeper inundation. The combination of lowering platform elevation by 10% and converting to a tidal flat (i.e., removing vegetation) had the largest impact on distance to complete attenuation of all of the scenarios, increasing on average by $583\% \pm 59\%$ (Figure 5). Compared to converting to a tidal flat and maintaining elevation, the added effect of lowering the elevation increases the distance to complete attenuation by $88\% \pm 12\%$ (Figure 5). Bottom roughness does attenuate waves but has a decreased impact in deeper water.

3.2.5. Lower Marsh Platform Elevation

Lowering the marsh platform by 10%, while still maintaining the vegetation, caused the waves to propagate farther inland for every transect and every storm simulation. Lowering the elevation creates greater inundation, meaning the vegetation takes up a smaller portion of the water column and has less impact on decreasing the wave height. For the example shown in Figure 7B, lowering (black line) led to a 45 m difference in distance for complete attenuation. Even though the same effect was observed elsewhere, the relative difference between distances required for complete attenuation changed depending on the hydrodynamic conditions. On average, the distance increased by $175\% \pm 9\%$ compared to the base case (Figure 5). The outcome of lowering elevation compared to removing vegetation (3.2.3) varied depending on location; 60% of transects required a shorter distance to complete attenuation with a lower elevation compared to removing vegetation, but those transects with the reverse outcome required much greater distances. On average, the distance required was $18\% \pm 10\%$ greater with a lower elevation compared to no vegetation (Figure 5).

3.2.6. Filling in Ditches

Filling ditches had a mixed effect on the wave heights depending on the width of the ditch, the number of ditches filled, and the hydrodynamic conditions, but this impact was consistently small. For the transects that were impacted by filling ditches, the median decrease in required distance was 3 m. Figure 7C shows an example with deeper and wider ditches, where filling in one ditch (about 150 m from the marsh edge) caused a 30 m difference in complete attenuation distance. On average, compared to the base case, the required distance to complete wave attenuation was decreased by $1\% \pm 1\%$ (Figure 5). For all scenarios except the conversion to *Sp. patens*, filling in ditches caused a decrease in the distance to complete wave attenuation (negative values in column 6 of Figure 5), with the greatest difference of $62\% \pm 3\%$ occurring when compared to conversion to a tidal flat with lower elevation.

Note, no transects ran parallel to the ditches, but rather, cut across them. Also, the inundation patterns were not altered in the model to reflect the lack of flow conveyance from filled ditches; therefore, there may be effects that were not captured.

4. Discussion

4.1. Incident Wave Energy a Function of Tidal Regime and SLR

Given strong winds, waves grow larger in deep water, which is why we see an increase in wave heights at the marsh edge for high tide versus low tide and with rising sea level. The latter finding assumes that sedimentation in the backbarrier basin does not keep up with rising sea level thereby deepening the water. For our study, the waves during a high-neap tide ("low tide" condition) were on average 44% larger with SLR compared to without SLR. This increase diminishes to 23% for waves during a high-spring tide ("high tide" condition). This finding implies that under the present conditions, wave energy, which is a

proxy for storm impact, is more dependent on tidal conditions (high versus low tide; spring versus neap tide) than it will be in future SLR scenarios in which sea level rises only 10's of centimeters. It is also noted that the difference between neap and spring-tidal elevation increases with increasing tidal range. Moreover, for Plum Island Sound where spring tidal ranges exceed 3 m, a fast-moving extratropical storm that produces a meter storm surge would produce waves having little effect at low tide, whereas that same storm impacting the marsh at high tide would create significant wave energies. Under these conditions, there would be close to a meter of water over the marsh platform, and thus the entirety of backbarrier flooding would generate much larger waves than under normal high-water conditions when much of the marsh is exposed [7]. In projecting the future of the marsh platform, it is forecasted that the Great Marsh will succumb to SLR and the *Spartina patens* high marsh will be transformed to *Spartina alterniflora* low marsh by 2070 [25].

4.2. Effects of Vegetation

The capacity of various plant species to attenuate waves is related to their resilience, flexibility, biomass, geographic extent, planting density, and arrangement [48–55]. For example, Cassalho et al. [56] investigated wave attenuation by *Phragmites australis* and *Spartina alterniflora* using bay-wide modeling scenarios. The authors found that *Phragmites australis*-dominated marshes can provide significantly more wave attenuation than native *Spartina alterniflora*-dominated marshes during extreme hurricane events due to their high biomass and rigidity. On the contrary, under high-frequency and low-intensity storm events, *Spartina alterniflora*-dominated marshes are slightly more efficient than invasive *Phragmites australis* marshes due to their high planting density. Despite the abundance of experimental studies documenting the influence of biophysical properties of saltmarsh plants on wave attenuation, few studies have used live coastal marsh vegetation (*P. maritima* [52,57–59]; *Spartina anglica*, [60,61]; *Elymus athericus* [52,59,60]; *Atriplex prostrata* [59]; *Spartina alterniflora* [62–64]; and *Juncus roemarianus* [65]) and additional research that develops knowledge of species-specific attenuation capacity is needed.

4.3. Shoreline Wave Heights Impacted by Loss of Elevation

The attenuation of wave energy across the marsh is a product of hydrodynamic conditions, characteristics of the vegetation, and the physiography of the marsh. When wave attenuation is projected into the future, these factors along with rates of relative SLR and the vertical accretion of the marsh surface must be considered. Several studies have investigated future levels of water on the marsh and how that will affect wave attenuation. For example, Hijuelos et al. [43] used two modeling schemes SLAMM (Sea Level Affecting Marshes Model [66,67]) and XBeach [68–70] to investigate sea level changes and wave attenuation, respectively, at marsh systems in coastal Louisiana and the Dutch Wadden Sea. For Louisiana, their modeling showed that rates of wave attenuation declined steadily up to year 30 and then rapidly decreased after year 40, indicating a critical threshold had been reached. In the case of the stable and high sediment supply Dutch Wadden Sea marshes, minimal changes in wave attenuation were recorded over the projected 50-year period through a variety of SLR and accretion scenarios [43]. In another study of San Francisco Bay marshes, Taylor-Burns et al. [71] used field data and XBeach non-hydrostatic mode (XB-NH; [72]), which incorporates different characteristics of the vegetation [70,73], to analyze the effects of increasing water levels on the marsh. They found that a decreasing impact to wave attenuation is a function of 1. offshore significant wave height, 2. drag coefficient, 3. water level, and 4. marsh width, and that the greatest reduction in H_S due to vegetation occurs with the largest waves and highest water levels. Foster-Martinez et al. [42] modeled wave attenuation differences for Hydro-MEM [74,75] landscapes under intermediate-high

and high SLR in Grand Bay, AL. The areas of wave influence for intermediate high were smaller than that for high SLR in 2050. This difference was primarily driven by differences in biomass productivity with the intermediate-high SLR case maintaining greater areas with high productivity biomass [42]. Other studies take the analysis further by including morphodynamics in the modeling framework. Chen et al. [21] and Marino et al. [22] calculated erosion reduction for scenarios with and without a nature-based solution intervention. Chen et al. [21] tested a range of seagrass meadow configurations, showing the importance of stem density and height to optimizing erosion reduction. Marino et al. [22] use a similar approach to test the addition of dune revegetation and a seagrass meadow reconstruction for a site in Italy with current and future environmental conditions. They found the positive impact of the interventions diminished with greater sea level rise. For the seagrass meadow erosion reduction efficiencies, the average across all transects decreased from 31% to 24% between current conditions and projections to 2100 (0.78 m SLR). Although, some transects had erosion reduction efficiencies greater than 50% with a seagrass meadow, showing the importance of site-specific conditions. The results of our study further underscore the importance of both vegetation and elevation to wave attenuation. Running the model with no vegetation led to an average distance to complete attenuation over five times longer, while running it with lower elevation and maintaining vegetation only led to an increase of about 2.5 times. Combining these effects and running with no vegetation with a lower elevation led to average distances nearly seven times larger compared to the base case, which was the greatest average difference in distance to complete attenuation of the scenarios tested.

4.4. Conservative Nature of Presented Modeling Approach

The conditions observed in the field were used to calibrate the model (i.e., set Equation (7), the C_D -Reynolds number relationship) and were less energetic than those modeled. The largest wave height modeled under base conditions was 0.63 m, while the maximum significant wave height in the field data used to calibrate Equation (7) was 0.45 m. We are confident that even with this difference, the modeled results are relatively conservative due to the method of setting the drag coefficient, C_D , and due to the timing of vegetation surveys, as discussed below.

Within MTWA, the C_D -Reynolds number relationship (Equation (7)) relies upon input from both the vegetation survey and the Delft3D model outputs. We use the orbital velocity, u_b , value calculated by Delft3D in open water at the start of the transect to calculate the Reynolds number, which is then used to calculate C_D . This C_D value is then used for the complete distance of the transect, even though as waves lose energy across the marsh, the orbital velocity decreases. Our field observations showed that orbital velocity decreased by about 75% (calculated from the pressure time series) over the 70 m transect. By using the u_b value from Delft3D in open water, we are overestimating the Reynolds number, and therefore, underestimating the C_D and wave attenuation. For example, a typical value of u_b in open water was 0.2 m/s, which, with our standard conditions, gives a C_D of 0.028, whereas a typical u_b at the end of a transect was 0.05 m/s, which, under the same standard conditions, gives a C_D of 1.167. The higher C_D value produces greater attenuation in a shorter distance. Using the u_b at the start of the transect to determine the C_D reduced the modeled wave attenuation. Even with this approach, the marsh was overall effective in removing wave energy.

4.5. Wave Transformation over Scarped Edges Is Not Well Constrained

Most of the marsh edges in the study site are scarps, which is not a well-understood transition regarding wave transformation. We relied on field observations (see Supplemental

Information) and created a relationship between attenuation and the depth at the top of the scarp normalized by the scarp height. Garzon et al. [76] took a similar approach and formulated a relationship between wave height before the marsh edge and wave attenuation for four classes based on the depth at the top of the scarp ranging from 0.55 to 0.90 m. The bounds of the depth conditions are not directly comparable since our observations are for less inundated conditions. However, in 0.55 m of water with a 1.4 m scarp, the empirical relationships show a similar result with a 0.3 m wave decreasing to 0.14 m and 0.18 m with the relationship presented here and in Garzon et al. [76], respectively. Additional measurements under a range of depth and scarp height conditions would help to understand the complex interactions between the wave processes at work (e.g., attenuation, shoaling, and reflection).

5. Conclusions

The marsh platform in the Great Marsh, MA, effectively reduces wave energy, and modeled wave heights were less than 0.1 m at all upland edges for the base case under the selected storms run at high-spring tide. Six environmental scenarios, in addition to SLR, were run to explore the attenuation capacity of the marsh changes. The largest reductions were seen with lowering the marsh platform elevation and removing vegetation. Compared to the base case, only conversion to all *Sp. patens* increased the wave attenuation capacity. Wave heights increased at the marsh edge with increasing inundation, either from the tidal case run or SLR. This study shows the relative change in the attenuation capacity of different environmental manipulations, allowing for better comparison between them, and it demonstrates how local conditions can produce outcomes that are not always expected.

Supplementary Materials: The following supporting information can be downloaded at <https://www.mdpi.com/article/10.3390/jmse13061188/s1> (References [77–79] are cited in the Supplementary Materials).

Author Contributions: Conceptualization, D.M.F., Z.J.H., I.Y.G. and A.N.; methodology, M.R.F.-M., I.Y.G. and M.M.S.; software, M.R.F.-M. and I.Y.G.; formal analysis, M.R.F.-M.; data curation, A.N., Z.J.H. and M.R.F.-M.; writing—original draft preparation, D.M.F., I.Y.G. and M.R.F.-M.; writing—review and editing, M.M.S., A.N., Z.J.H., I.Y.G., D.M.F. and M.R.F.-M.; visualization, M.R.F.-M.; funding acquisition, D.M.F., Z.J.H. and I.Y.G. All authors have read and agreed to the published version of the manuscript.

Funding: This research was funded by the State of Massachusetts Department of Energy and Environmental Affairs Municipal Vulnerability Preparedness Grant Program. award RFR ENV 18 POL 04 to the Town of Newbury.

Data Availability Statement: The original contributions presented in this study are included in the article, Supplementary Information, and field observations and model code repositories [80,81]. Further inquiries can be directed to the corresponding author.

Acknowledgments: The authors would like to thank Geoffrey Walker for involvement with the Town of Newbury and Francesca Messina for assistance with figures. The manuscript greatly benefitted from two anonymous reviews.

Conflicts of Interest: The authors declare no conflicts of interest. The funders had no role in the design of the study; in the collection, analyses, or interpretation of data; in the writing of the manuscript; or in the decision to publish the results.

References

1. Shepard, C.C.; Crain, C.M.; Beck, M.W. The Protective Role of Coastal Marshes: A Systematic Review and Meta-Analysis. *PLoS ONE* **2011**, *6*, e27374. [[CrossRef](#)] [[PubMed](#)]
2. Resio, D.T.; Westerink, J.J. Modeling the Physics of Storm Surges. *Phys. Today* **2008**, *61*, 33–38. [[CrossRef](#)]

3. Mcowen, C.; Weatherdon, L.; Bochove, J.-W.; Sullivan, E.; Blyth, S.; Zockler, C.; Stanwell-Smith, D.; Kingston, N.; Martin, C.; Spalding, M.; et al. A Global Map of Saltmarshes. *Biodivers. Data J.* **2017**, *5*, e11764. [CrossRef]
4. Petry, M.; Rogers, D. Nor'easter Slams into Greater Newburyport. *The Daily News*, 4 April 2024.
5. Colle, B.A.; Zhang, Z.; Lombardo, K.A.; Chang, E.; Liu, P.; Zhang, M. Historical Evaluation and Future Prediction of Eastern North American and Western Atlantic Extratropical Cyclones in the CMIP5 Models during the Cool Season. *J. Clim.* **2013**, *26*, 6882–6903. [CrossRef]
6. Zhang, Z.; Colle, B.A. Impact of Dynamically Downscaling Two CMIP5 Models on the Historical and Future Changes in Winter Extratropical Cyclones along the East Coast of North America. *J. Clim.* **2018**, *31*, 8499–8525. [CrossRef]
7. FitzGerald, D.M.; Hughes, Z.J.; Georgiou, I.Y.; Black, S.; Novak, A. Enhanced, Climate-Driven Sedimentation on Salt Marshes. *Geophys. Res. Lett.* **2020**, *47*, e2019GL086737. [CrossRef]
8. Leonardi, N.; Fagherazzi, S. How Waves Shape Salt Marshes. *Geology* **2014**, *42*, 887–890. [CrossRef]
9. Leonardi, N.; Carnacina, I.; Donatelli, C.; Ganju, N.K.; Plater, A.J.; Schuerch, M.; Temmerman, S. Dynamic Interactions between Coastal Storms and Salt Marshes: A Review. *Geomorphology* **2018**, *301*, 92–107. [CrossRef]
10. Houttuijn Bloemendaal, L.J.; FitzGerald, D.M.; Hughes, Z.J.; Novak, A.B.; Phippen, P. What Controls Marsh Edge Erosion? *Geomorphology* **2021**, *386*, 107745. [CrossRef]
11. Bloemendaal, L.J.H.; FitzGerald, D.M.; Hughes, Z.J.; Novak, A.B.; Georgiou, I.Y. Reevaluating the Wave Power-Salt Marsh Retreat Relationship. *Sci. Rep.* **2023**, *13*, 2884. [CrossRef]
12. Moeller, I.; Spencer, T.; French, J.R. Wind Wave Attenuation over Saltmarsh Surfaces: Preliminary Results from Norfolk, England. *J. Coast. Res.* **1996**, *12*, 1009–1016.
13. Foster-Martinez, M.R.; Lacy, J.R.; Ferner, M.C.; Variano, E.A. Wave Attenuation across a Tidal Marsh in San Francisco Bay. *Coast. Eng.* **2018**, *136*, 26–40. [CrossRef]
14. Feagin, R.A.; Innocenti, R.A.; Bond, H.; Wengrove, M.; Huff, T.P.; Lomonaco, P.; Tsai, B.; Puleo, J.; Pontiki, M.; Figlus, J.; et al. Does Vegetation Accelerate Coastal Dune Erosion during Extreme Events? *Sci. Adv.* **2023**, *9*, eadg7135. [CrossRef]
15. NOAA National Oceanic and Atmospheric Administration. Available online: <https://tidesandcurrents.noaa.gov/stationhome.html?id=8419870> (accessed on 1 June 2018).
16. Vallino, J.J.; Hopkinson, C.S., Jr. Estimation of Dispersion and Characteristic Mixing Times in Plum Island Sound Estuary. *Estuar. Coast. Shelf Sci.* **1998**, *46*, 333–350. [CrossRef]
17. Zhao, L.; Chen, C.; Vallino, J.; Hopkinson, C.; Beardsley, R.C.; Lin, H.; Lerczak, J. Wetland-estuarine-shelf Interactions in the Plum Island Sound and Merrimack River in the Massachusetts Coast. *J. Geophys. Res. Ocean.* **2010**, *115*, 2009JC006085. [CrossRef]
18. Wilson, C.A.; Hughes, Z.J.; FitzGerald, D.M.; Hopkinson, C.S.; Valentine, V.; Kolker, A.S. Saltmarsh Pool and Tidal Creek Morphodynamics: Dynamic Equilibrium of Northern Latitude Saltmarshes? *Geomorphology* **2014**, *213*, 99–115. [CrossRef]
19. Valentine, V.; Hopkinson, C., Jr. NCALM LIDAR: Plum Island, Massachusetts, USA: 18–19 April 2005. Elevation data and products produced by NSF-Supported National Center for Airborne Laser Mapping (NCALM) for Plum Island Ecosystems Long Term Ecological Research (PIE-LTER) Project. 2005. Available online: <https://portal.edirepository.org/nis/metadataviewer?packageid=knb-lter-pie.422.1> (accessed on 1 June 2018).
20. Millette, T.L.; Argow, B.A.; Marcano, E.; Hayward, C.; Hopkinson, C.S.; Valentine, V. Salt Marsh Geomorphological Analyses via Integration of Multitemporal Multispectral Remote Sensing with LIDAR and GIS. *J. Coast. Res.* **2010**, *265*, 809–816. [CrossRef]
21. Chen, W.; Staneva, J.; Jacob, B.; Sánchez-Artús, X.; Wurpts, A. What-If Nature-Based Storm Buffers on Mitigating Coastal Erosion. *Sci. Total Environ.* **2024**, *928*, 172247. [CrossRef]
22. Marino, M.; Nasca, S.; Alkharoubi, A.I.; Cavallaro, L.; Foti, E.; Musumeci, R.E. Efficacy of Nature-Based Solutions for Coastal Protection under a Changing Climate: A Modelling Approach. *Coast. Eng.* **2025**, *198*, 104700. [CrossRef]
23. Cooperative Institute for Research in Environmental Sciences. *Continuously Updated Digital Elevation Model (CUDEM)—1/9 Arc-Second Resolution Bathymetric-Topographic Tiles*; Cooperative Institute for Research in Environmental Sciences: Boulder, CO, USA, 2014.
24. OCM Partners 2014 USACE NAE Topobathy Lidar DEM: Newbury, MA, USA. Available online: <https://www.fisheries.noaa.gov/inport/item/64731> (accessed on 1 June 2018).
25. FitzGerald, D.M.; Hein, C.J.; Connell, J.E.; Hughes, Z.J.; Georgiou, I.Y.; Novak, A.B. Largest Marsh in New England near a Precipice. *Geomorphology* **2021**, *379*, 107625. [CrossRef]
26. Shi, F.; Kirby, J.T.; Harris, J.C.; Geiman, J.D.; Grilli, S.T. A High-Order Adaptive Time-Stepping TVD Solver for Boussinesq Modeling of Breaking Waves and Coastal Inundation. *Ocean. Model.* **2012**, *43–44*, 36–51. [CrossRef]
27. Shi, F.; Malej, M.; Smith, J.M.; Kirby, J.T. Breaking of Ship Bores in a Boussinesq-Type Ship-Wake Model. *Coast. Eng.* **2018**, *132*, 1–12. [CrossRef]
28. Kirby, J.T. Chapter 1 Boussinesq Models and Applications to Nearshore Wave Propagation, Surf Zone Processes and Wave-Induced Currents. In *Elsevier Oceanography Series*; Elsevier: Amsterdam, The Netherlands, 2003; Volume 67, pp. 1–41, ISBN 978-0-444-51149-2.

29. Collins, P.; MacMahan, J.; Thornton, E.; Benbow, C.; Jessen, P. Beach and Backward Bragg Sea-Swell Wave Reflection Across Rocky and Sandy Shores. *J. Geophys. Res. Ocean.* **2024**, *129*, e2023JC020177. [[CrossRef](#)]
30. Xu, W.; Chen, C.; Htet, M.H.; Sarkar, M.S.I.; Tao, A.; Wang, Z.; Fan, J.; Jiang, D. Experimental Investigation on Bragg Resonant Reflection of Waves by Porous Submerged Breakwaters on a Horizontal Seabed. *Water* **2022**, *14*, 2682. [[CrossRef](#)]
31. Gao, J.; Ma, X.; Dong, G.; Chen, H.; Liu, Q.; Zang, J. Investigation on the Effects of Bragg Reflection on Harbor Oscillations. *Coast. Eng.* **2021**, *170*, 103977. [[CrossRef](#)]
32. Lesser, G.R.; Roelvink, J.A.; van Kester, J.A.T.M.; Stelling, G.S. Development and Validation of a Three-Dimensional Morphological Model. *Coast. Eng.* **2004**, *51*, 883–915. [[CrossRef](#)]
33. Booij, N.; Ris, R.C.; Holthuijsen, L.H. A Third-generation Wave Model for Coastal Regions: 1. Model Description and Validation. *J. Geophys. Res. Ocean.* **1999**, *104*, 7649–7666. [[CrossRef](#)]
34. Hanegan, K.C.; FitzGerald, D.M.; Georgiou, I.Y.; Hughes, Z.J. Long-Term Sea Level Rise Modeling of a Basin-Tidal Inlet System Reveals Sediment Sinks. *Nat. Commun.* **2023**, *14*, 7117. [[CrossRef](#)]
35. Georgiou, I.Y.; Messina, F.; Sakib, M.M.; Zou, S.; Foster-Martinez, M.; Bregman, M.; Hein, C.J.; Fenster, M.S.; Shawler, J.L.; McPherran, K.; et al. Hydrodynamics and Sediment-Transport Pathways along a Mixed-Energy Spit-Inlet System: A Modeling Study at Chincoteague Inlet (Virginia, USA). *J. Mar. Sci. Eng.* **2023**, *11*, 1075. [[CrossRef](#)]
36. Sullivan, J.C.; Torres, R.; Garrett, A.; Blanton, J.; Alexander, C.; Robinson, M.; Moore, T.; Amft, J.; Hayes, D. Complexity in Salt Marsh Circulation for a Semienclosed Basin. *J. Geophys. Res. Earth Surf.* **2015**, *120*, 1973–1989. [[CrossRef](#)]
37. Liu, K.; Chen, Q.; Hu, K.; Xu, K.; Twilley, R.R. Modeling Hurricane-Induced Wetland-Bay and Bay-Shelf Sediment Fluxes. *Coast. Eng.* **2018**, *135*, 77–90. [[CrossRef](#)]
38. Caldwell, R.L.; Edmonds, D.A. The Effects of Sediment Properties on Deltaic Processes and Morphologies: A Numerical Modeling Study. *J. Geophys. Res. Earth Surf.* **2014**, *119*, 961–982. [[CrossRef](#)]
39. Mukai, A.Y.; Westerink, J.J.; Luettich, R.A. *Guidelines for Using Eastcoast 2001 Database of Tidal Constituents Within Western North Atlantic Ocean, Gulf of Mexico and Caribbean Sea*; US Army Engineer Research and Development Center, Coastal and Hydraulics Laboratory: Vicksburg, MS, USA, 2002.
40. Cialone, M.A.; Bocamazo, L.M.; Nadal-Caraballo, N.C.; Massey, T.C.; Melby, J.A. North Atlantic Coast Comprehensive Study (Naccs) Storm Simulation and Statistical Analysis: Part I—Overview. In *The Proceedings of the Coastal Sediments 2015*; World Scientific: San Diego, CA, USA, 2015.
41. USACE (US Army Corps of Engineers). *Wave Information Study (WIS)*; USACE: Wiesbaden, Germany, 2023.
42. Foster-Martinez, M.R.; Alizad, K.; Hagen, S.C. Estimating Wave Attenuation at the Coastal Land Margin with a GIS Toolbox. *Environ. Model. Softw.* **2020**, 104788. [[CrossRef](#)]
43. Hijuelos, A.C.; Dijkstra, J.T.; Carruthers, T.J.B.; Heynert, K.; Reed, D.J.; van Wesenbeeck, B.K. Linking Management Planning for Coastal Wetlands to Potential Future Wave Attenuation under a Range of Relative Sea-Level Rise Scenarios. *PLoS ONE* **2019**, *14*, e0216695. [[CrossRef](#)]
44. Dean, R.G.; Dalrymple, R.A. *Water Wave Mechanics for Engineers and Scientists*; World Scientific Publishing Co., Inc.: Singapore, 1991; Volume 2.
45. Nielsen, P. *Coastal Bottom Boundary Layers and Sediment Transport*; World Scientific Publishing Co., Inc.: Singapore, 1992; Volume 4.
46. Kopp, R.E.; Kemp, A.C.; Bittermann, K.; Horton, B.P.; Donnelly, J.P.; Gehrels, W.R.; Hay, C.C.; Mitrovica, J.X.; Morrow, E.D.; Rahmstorf, S. Temperature-Driven Global Sea-Level Variability in the Common Era. *Proc. Natl. Acad. Sci. USA* **2016**, *113*, E1434–E1441. [[CrossRef](#)]
47. Donnelly, J.P.; Bertness, M.D. Rapid Shoreward Encroachment of Salt Marsh Cordgrass in Response to Accelerated Sea-Level Rise. *Proc. Natl. Acad. Sci.* **2001**, *98*, 14218–14223. [[CrossRef](#)]
48. Maza, M.; Lara, J.L.; Losada, I.J. Experimental Analysis of Wave Attenuation and Drag Forces in a Realistic Fringe Rhizophora Mangrove Forest. *Adv. Water Resour.* **2019**, *131*, 103376. [[CrossRef](#)]
49. Augustin, L.N.; Irish, J.L.; Lynett, P. Laboratory and Numerical Studies of Wave Damping by Emergent and Near-Emergent Wetland Vegetation. *Coast. Eng.* **2009**, *56*, 332–340. [[CrossRef](#)]
50. Anderson, M.E.; Smith, J.M. Wave Attenuation by Flexible, Idealized Salt Marsh Vegetation. *Coast. Eng.* **2014**, *83*, 82–92. [[CrossRef](#)]
51. Blackmar, P.J.; Cox, D.T.; Wu, W.-C. Laboratory Observations and Numerical Simulations of Wave Height Attenuation in Heterogeneous Vegetation. *J. Waterw. Port Coast. Ocean. Eng.* **2014**, *140*, 56–65. [[CrossRef](#)]
52. Rupperecht, F.; Möller, I.; Paul, M.; Kudella, M.; Spencer, T.; van Wesenbeeck, B.K.; Wolters, G.; Jensen, K.; Bouma, T.J.; Miranda-Lange, M.; et al. Vegetation-Wave Interactions in Salt Marshes under Storm Surge Conditions. *Ecol. Eng.* **2017**, *100*, 301–315. [[CrossRef](#)]
53. Ozeren, Y.; Wren, D.G.; Wu, W. Experimental Investigation of Wave Attenuation through Model and Live Vegetation. *J. Waterw. Port Coast. Ocean Eng.* **2014**, *140*, 04014019. [[CrossRef](#)]

54. Paul, K.I.; Roxburgh, S.H.; Chave, J.; England, J.R.; Zerihun, A.; Specht, A.; Lewis, T.; Bennett, L.T.; Baker, T.G.; Adams, M.A.; et al. Testing the Generality of Above-ground Biomass Allometry across Plant Functional Types at the Continent Scale. *Glob. Change Biol.* **2016**, *22*, 2106–2124. [CrossRef]
55. Van Veelen, T.J.; Fairchild, T.P.; Reeve, D.E.; Karunaratna, H. Experimental Study on Vegetation Flexibility as Control Parameter for Wave Damping and Velocity Structure. *Coast. Eng.* **2020**, *157*, 103648. [CrossRef]
56. Cassalho, F.; De Lima, A.D.S.; Coleman, D.J.; Henke, M.; Miesse, T.W.; Coelho, G.D.A.; Ferreira, C.M. Projecting Future Wave Attenuation by Vegetation from Native and Invasive Saltmarsh Species in the United States. *Reg. Stud. Mar. Sci.* **2023**, *68*, 103264. [CrossRef]
57. Lara, J.L.; Maza, M.; Ondiviela, B.; Trinogga, J.; Losada, I.J.; Bouma, T.J.; Gordejuela, N. Large-Scale 3-D Experiments of Wave and Current Interaction with Real Vegetation. Part 1: Guidelines for Physical Modeling. *Coast. Eng.* **2016**, *107*, 70–83. [CrossRef]
58. Maza, M.; Lara, J.L.; Losada, I.J. Tsunami Wave Interaction with Mangrove Forests: A 3-D Numerical Approach. *Coast. Eng.* **2015**, *98*, 33–54. [CrossRef]
59. Möller, I.; Kudella, M.; Rupprecht, F.; Spencer, T.; Paul, M.; van Wesenbeeck, B.K.; Wolters, G.; Jensen, K.; Bouma, T.J.; Miranda-Lange, M.; et al. Wave Attenuation over Coastal Salt Marshes under Storm Surge Conditions. *Nat. Geosci* **2014**, *7*, 727–731. [CrossRef]
60. Paul, M.; Kerpen, N.B. Erosion Protection by Winter State of Salt Marsh Vegetation. *J. Ecohydraul.* **2022**, *7*, 144–153. [CrossRef]
61. Poppema, D.W.; Willemsen, P.W.; de Vries, M.B.; Zhu, Z.; Borsje, B.W.; Hulscher, S.J. Experiment-Supported Modelling of Salt Marsh Establishment. *Ocean. Coast. Manag.* **2019**, *168*, 238–250. [CrossRef]
62. Knutson, P.L.; Brochu, R.A.; Seelig, W.N.; Inskeep, M. Wave Damping in *Spartina alterniflora* Marshes. *Wetlands* **1982**, *2*, 87–104. [CrossRef]
63. Jadhav, R.S.; Chen, Q. Field Investigation of Wave Dissipation over Salt Marsh Vegetation During Tropical Cyclone. *Int. Conf. Coastal. Eng.* **2012**, *1*, 41. [CrossRef]
64. Paquier, A.-E.; Haddad, J.; Lawler, S.; Ferreira, C.M. Quantification of the Attenuation of Storm Surge Components by a Coastal Wetland of the US Mid Atlantic. *Estuaries Coasts* **2016**, *40*, 930–946. [CrossRef]
65. Wu, W.; Ozeren, Y.; Wren, D.; Chen, Q.; Zhang, G.; Holland, M.; Ding, Y.; Kuiry, S.; Zhang, M.; Jadhav, R.; et al. *SERRI Project: Investigations of Surge and Wave Reduction by Vegetation*; SERRI Report 80037-01; National Center for Computational Hydroscience and Engineering, University of Mississippi: Oxford, MS, USA, 2011.
66. Park, R.A.; Armentano, T.V.; Cloonan, C.L. Predicting the Effects of Sea Level Rise on Coastal Wetlands. *Eff. Changes Stratos. Ozone Glob. Clim.* **1986**, *4*, 129–152.
67. Clough, J.; Park, R.A.; Fuller, R. *SLAMM 6 Beta Technical Documentation*; Warren Pinnacle: Waitsfield, VT, USA, 2010; p. 49.
68. Bolle, A.; Mercelis, P.; Roelvink, D.; Haerens, P.; Trouw, K. Application and Validation of XBeach for Three Different Field Sites. *Coast. Eng. Proc.* **2011**, *1*, 40. [CrossRef]
69. Harley, M.; Armaroli, C.; Ciavola, P. Evaluation of XBeach Predictions for a Real-Time Warning System in Emilia-Romagna, Northern Italy. *J. Coast. Res.* **2011**, 1861–1865. Available online: <https://www.jstor.org/stable/26482499> (accessed on 25 April 2025).
70. van Rooijen, A.A.; van Thiel de Vries, J.S.M.; McCall, R.T.; van Dongeren, A.R.; Roelvink, J.A.; Reniers, A.J.H.M. Modeling of Wave Attenuation by Vegetation with XBeach. In Proceedings of the E-Proceedings of the 36th IAHR World Congress, The Hague, The Netherlands, 28 June–3 July 2015; IAHR: Madrid, Spain, 2015; Volume 2016, p. 6.
71. Taylor-Burns, R.; Nederhoff, K.; Lacy, J.R.; Barnard, P.L. The Influence of Vegetated Marshes on Wave Transformation in Sheltered Estuaries. *Coast. Eng.* **2023**, *184*, 104346. [CrossRef]
72. de Ridder, M.P.; Smit, P.B.; van Dongeren, A.R.; McCall, R.T.; Nederhoff, K.; Reniers, A.J. Efficient Two-Layer Non-Hydrostatic Wave Model with Accurate Dispersive Behaviour. *Coast. Eng.* **2021**, *164*, 103808. [CrossRef]
73. Van Rooijen, A.; McCall, R.; Van Thiel de Vries, J.; Van Dongeren, A.; Reniers, A.; Roelvink, J. Modeling the Effect of Wave-Vegetation Interaction on Wave Setup. *J. Geophys. Res. Ocean.* **2016**, *121*, 4341–4359. [CrossRef]
74. Alizad, K.; Hagen, S.C.; Morris, J.T.; Bacopoulos, P.; Bilskie, M.V.; Weishampel, J.F.; Medeiros, S.C. A Coupled, Two-Dimensional Hydrodynamic-Marsh Model with Biological Feedback. *Ecol. Model.* **2016**, *327*, 29–43. [CrossRef]
75. Alizad, K.; Hagen, S.C.; Medeiros, S.C.; Bilskie, M.V.; Morris, J.T.; Balthis, L.; Buckel, C.A. Dynamic Responses and Implications to Coastal Wetlands and the Surrounding Regions under Sea Level Rise. *PLoS ONE* **2018**, *13*, e0205176. [CrossRef] [PubMed]
76. Garzon, J.L.; Maza, M.; Ferreira, C.M.; Lara, J.L.; Losada, I.J. Wave Attenuation by *Spartina* Saltmarshes in the Chesapeake Bay under Storm Surge Conditions. *J. Geophys. Res. Ocean.* **2019**, *124*, 5220–5243. [CrossRef]
77. Wiberg, P.L.; Sherwood, C.R. Calculating Wave-Generated Bottom Orbital Velocities from Surface-Wave Parameters. *Comput. Geosci.* **2008**, *34*, 1243–1262. [CrossRef]
78. Kobayashi, N.; Raichle, A.W.; Asano, T. Wave Attenuation by Vegetation. *J. Waterw. Port Coast. Ocean Eng.* **1993**, *119*, 30–48. [CrossRef]
79. Mendez, F.J.; Losada, I.J. An Empirical Model to Estimate the Propagation of Random Breaking and Nonbreaking Waves over Vegetation Fields. *Coast. Eng.* **2004**, *51*, 103–118. [CrossRef]

80. Foster-Martinez, M.; FitzGerald, D.; Georgiou, I.; Hughes, Z. Assessing Storm Energy Reduction by the Vegetated Salt Marsh Platform in Newbury, MA, Pressure Timeseries. *Zenodo* 2025. [[CrossRef](#)]
81. Foster-Martinez, M.; Georgiou, I. Marsh Transect Wave Attenuation (MTWA) Model. *Zenodo* 2025. [[CrossRef](#)]

Disclaimer/Publisher's Note: The statements, opinions and data contained in all publications are solely those of the individual author(s) and contributor(s) and not of MDPI and/or the editor(s). MDPI and/or the editor(s) disclaim responsibility for any injury to people or property resulting from any ideas, methods, instructions or products referred to in the content.